Nanoclay Distribution and Its Influence on the Mechanical Properties of Rubber Blends

Abhijit Bandyopadhyay, Varun Thakur, Sudip Pradhan, Anil K. Bhowmick

Rubber Technology Centre, Indian Institute of Technology, Kharagpur 721302, India

Received 4 September 2008; accepted 27 April 2009
DOI 10.1002/app.30655
Published online 17 September 2009 in Wiley InterScience (www.interscience.wiley.com).

ABSTRACT: The distribution of modified and unmodified nanoclays inside the rubber phases of immiscible rubber–rubber blends composed of nonpolar–polar natural rubber (NR)/epoxidized natural rubber (ENR) and nonpolar–nonpolar NR/polybutadiene rubber (BR) was investigated for the first time. The distribution of clays at various loadings in the blends was calculated from the viscoelastic properties of the blends. For example, in the 50 : 50 NR/ENR blend, 42% Cloisite 30B migrated to the NR phase, and 58% went to the ENR phase. However, in the same blend, only 7% Cloisite Na^+ was found in the NR phase, and 93% was found in the ENR phase. Again, in the 50 : 50 NR/BR blends, the NR phase contained 85% Cloisite 30B, whereas 55% Cloisite Na^+ migrated to the NR phase. All these observations were explained with the help of viscosity, X-ray diffraction, and morphology analyses. The effect of the distribution of the clay on the mechanical properties was also discussed. © 2009 Wiley Periodicals, Inc. J Appl Polym Sci 115: 1237–1246, 2010

Key words: blends; elastomers; mechanical properties; nanocomposites; rubber

INTRODUCTION

Nanocomposites are defined as materials in which the particle size of dispersed filler is in the nanometer range in at least one dimension. The synthesis and characterization of organic–inorganic nanocomposites composed of an organic polymer matrix and inorganic filler dispersants have been a subject of investigation in recent years.[1,2] That may be attributed to the superiority of the mechanical properties,[3–11] barrier effect,[12,13] flame retardancy,[14–18] and thermochemical stability of the nanocomposites.[19] The two most popular categories of nanofillers extensively studied have been the zero-dimensional metal oxides and the one-dimensional nanoclay/layered silicates. Two idealized morphologies can be seen with nanosilicate fillers in the postdispersion stage in polymers: (1) exfoliated (i.e., the silicate layers are totally delaminated and disordered) and (2) intercalated (i.e., the silicate layers are partially separated by polymer chains, but an ordered structure is still retained).

In a ideal nanocomposite, the clay layers must be uniformly dispersed and exfoliated in the polymer matrix rather than being aggregated as tactoids. However, in all practical instances, nanocomposites having both exfoliated and intercalated morphologies have been obtained. It is superfluous to say that the properties of nanocomposites are a function of their morphology.

Montmorillonite, a layered clay mineral that belongs to the general family of 2 : 1 phyllosilicates, can undergo intercalation. It is the most extensively used layered silicate because of its natural occurrence and other beneficial properties, such as a high cation-exchange capacity, high surface area, and an obviously large aspect ratio. These layered silicates are hydrophilic in nature because of the presence of alkali and alkaline earth metal cations and surface silanol groups. To increase the hydrophobicity and compatibility with polymers, their cation-exchange capacity has been explored. Mainly, the Na^+ ion in the clay is exchanged with comparatively large alkyl ammonium (termed *onium*) ions, where the organic moiety attached to the amine helps in the development of organophilicity in the clay minerals. Two different clays, namely, Cloisite 30B (30B) and Cloisite Na^+ (NA), have been used to study the effect of clay variation in rubber–rubber blends.

Numerous polymer/layered silicate hybrid nanocomposites have been developed and characterized up to this point; some have been commercialized as well. Notable investigations have been published by Sinha Ray and Okamoto,[20] Kocsis and Wu,[21] Vaia et al.,[22] Giannelis,[23] Bandyopadhyay et al.,[24] and Bhattacharya et al.[25] on this topic. Also, previous investigations from our laboratory have covered rubber–clay

Correspondence to: A. K. Bhowmick (anilkb@rtc.iitkgp.ernet.in).

nanocomposites with various rubbery polymers, such as styrene–butadiene rubber,[3,26] nitrile rubber,[4] fluoroelastomers,[27] butyl rubber,[28] and Engage.[29]

In this study, we tried to explore the distribution of nanoclay in rubber–rubber immiscible blends and also its effect on the overall properties of the resultant nanocomposites. The variables were the rubber type (polar and nonpolar), the nature of the clays, the clay concentrations, and the blend compositions. This article has been divided into two parts for comprehensive representation of the results. The first part deals with the studies of the natural rubber (NR)/epoxidized natural rubber (ENR) blends, and the second part reports on the NR/polybutadiene rubber (BR) blends. Published reports on homopolymer–clay nanocomposites from NR, ENR, and BR are all available in the literature.[30–32] Solution blending and melt blending are known to be used for nanocomposite synthesis, but for commercial and environmental reasons, melt blending was used in this study.

EXPERIMENTAL

Materials

NR (ISNR-5; density = 0.92 g/cm^3, Mooney viscosity ML_{1+4} at 100°C = 36 after 5 min of mastication) was generously supplied by the Rubber Board (Kottayam, India). Epoxidized natural rubber with 50 mol % epoxy (ENR-50; density = 1.03 g/cm^3, Mooney viscosity ML_{1+4} at 100°C = 23 after 5 min of mastication) was obtained from Packwell Industries (Churu, India). BR (density = 0.93 g/cm^3, Mooney viscosity ML_{1+4} at 100°C = 50 after 5 min of mastication) was procured from IPCL (Baroda, India). The nanoclays—NA and 30B (30B contained 90 mequiv of quaternary ammonium ions/100 g of clay)—were purchased from Southern Clay Products (Gonzales, TX). The quaternary ammonium ion had a structure of $N^+(CH_2CH_2OH)_2(CH_3)T$ (where T represents an alkyl group that is ca. 65% C_{18}, 30% C_{16}, and 5% C_{14} for 30B).

Preparation of the rubber–clay nanocomposites

We made the NR/ENR-50 blends (75 : 25, 50 : 50, and 25 : 75 w/w) by blending the two rubbers in a laboratory-size (13″ × 6″) two-roll open mill (Schawabenthan, Berlin, Germany) with a tight nip gap (~ 1 mm) under identical conditions of time (~ 10 min), temperature (25°C), and friction ratio (1 : 1.15) for all of the mixes. The mixing time for similar compositions of the NR/BR blends at the same temperature and friction ratio was 8 min. The Mooney viscosity values of the individual rubbers (under identical conditions) were measured just after they were taken out from the two-roll open mill and are listed in Table I. Calculated amounts of the blends were further mixed for 2 min in a Haake Rheomix (Thermo Fisher Scientific, Karlsruhe, Germany) (with a fill factor of 0.7) at a temperature of 100°C at 60 rpm to obtain a better blend compatibility. Afterward, specified amounts of different nanoclays were melt-mixed at 100°C at a rotor speed of 60 rpm for another 4 min. The total mixing time in the Haake Rheomix was 6 (2 + 4) min. 30B was added in 2-, 4-, and 8-phr (1.01, 2.02, and 4.04 vol %, respectively) concentrations with respect to 100 parts of the blends; the comparison with NA was made at a 4-phr (1.4 vol %) concentration. The melt-blended rubber–clay lumps were immediately taken out of the intermix, and molded sheets about 1 mm thick were prepared after they were molded in a David Bridge press (Rockdale, UK) for 6 min at 100°C by the application of 5 MPa of pressure. All of the sheets were allowed to mature for 24 h before characterization.

TABLE I
Mooney Viscosity (ML_{1+4} at 100°C) Results for NR, ENR-50, and BR Just After Mastication in a Two-Roll Open Mill with a Tight Nip Gap (~ 1 mm) at 25°C

	Mooney viscosity		
Time (min)	NR	ENR	BR
0	55	37	70
1	42	28	58
2	39	26	54
3	38	24	52
4	36	23	50

Methods of characterization

X-ray diffraction (XRD) studies

XRD was used to characterize the nature and extent of the dispersions of the clays in the filled samples. XRD studies were performed with a Philips X-Pert Pro diffractometer (Royal Philips Electronics, Amsterdam, The Netherlands) in the range 2–10° with a copper target (λ = 0.154 nm). A tube voltage of 40 kV and a tube current of 30 mA were used for all of the samples. Bragg's law was used to compute the crystallographic spacing (d) of the clay layers.

Atomic force microscopy (AFM) studies

The morphology of the representative filled samples was obtained from a Multi Mode Scanning Probe Microscope model with a Nanoscope IIIa controller from Digital Instruments, Inc. (Veeco Metrology Group, Santa Barbara, CA). A tapping mode etched silicone probe (LTESP, with a spring constant of 48 N/m) with a resonance frequency of 190 kHz at 25°C was used. Height and phase images were recorded simultaneously at the resonance frequency

of the cantilever with a scan rate of 1 Hz and a resolution of 512 pixels in each (*x*,*y*) direction.

Dynamic mechanical analysis (DMA)

A DMA Q-800 dynamic mechanical analyzer from TA Instruments (Newcastle, DE) was used in tension mode in the temperature range −80 to 0°C at a frequency of 1 Hz and a heating rate of 2°C/min. The loss tangent (tan δ) values were measured as a function of temperature for all of the specimens under identical conditions. Three replicates were run for each dynamic modulus value.

Mechanical properties

The tensile and tear properties of the nanocomposites were measured with a Zwick/Roell-Z010 Ulm, Germany tensile tester machine for each composition at a strain rate of 500 mm/min under ambient conditions (25°C). The results were the averages of three readings.

RESULTS AND DISCUSSION

NR/ENR–clay hybrid composites

XRD

Figure 1(a) represents the X-ray diffractograms for the 50 : 50 NR/ENR-50 blend with various 30B contents (0, 2, 4, and 8 phr). The diffractogram for 30B is also shown in the same figure for comparison.

The modification of NA to 30B by the exchange of the interlayer cations with alkyl ammonium ions increased the interlayer spacing from 1.16 to 1.85 nm. The diffraction peak for 30B appeared at $2\theta \approx 4.78°$. In the nanocomposites, there was no distinct peak observed for 30B, especially at low concentrations (2–4 phr). This indicated predominant delamination of the clay tactoids into independent clay sheets. In all the cases, the diffraction peak due to the (001) plane was missing; this provided strong evidence for the insertion of the elastomers into the silicate galleries with the disruption of the stacked structure of 30B and gave a predominantly exfoliated morphology. Figure 1(b) shows the XRD patterns for the 50 : 50 NR/ENR-50 blends containing 4-phr 30B and NA, respectively. The diffraction peaks assigned to NA at 4.25, 5.00 (very small), and 6.00° were sharper than those of 30B and are clearly shown in the figure. Also, they appeared at a higher diffraction angle. This was probably due to the low gallery spacing in NA and its hydrophilicity, which prohibited extensive delamination, unlike in 30B. Figure 1(c) shows the X-ray analysis of different NR/ENR blends with 4 parts of 30B. The blend containing a higher proportion of NR showed more prominent clay peaks compared to the other compositions. This was probably due to slight aggregation of the modified clays and inferior dispersion in NR, which was the major phase in this case.

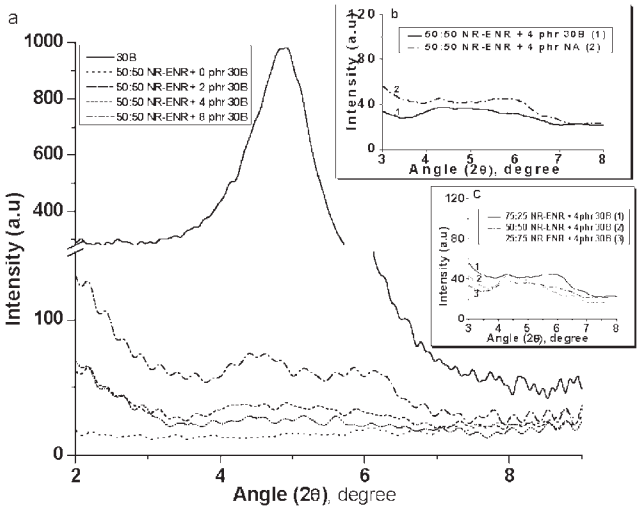

Figure 1 XRD patterns for (a) 50 : 50 NR/ENR-50 blends containing 0, 2, 4, or 8 phr 30B, (b) 50 : 50 NR/ENR-50 blends containing 4 phr 30B and NA, and (c) blends of various ratios with a constant 30B content (4 phr).

Morphological study

Figure 2(a–c) displays the AFM images of the hybrids containing both modified and unmodified clays in 50 : 50 rubber blends. In the tapping mode, the measurement of the difference between the phase angle of the excitation signal and the phase angle of the cantilever response was used to map compositional variations, such as stiffness, hardness, and viscoelasticity, on the sample surface. The dark-colored phase in the phase image was due to the lower modulus rubber in the blend, which may have been due to the deeper indentation of the cantilever in the sample. The distinct white features were the harder clay particles[33] observed in all of the pictures.

Figure 2(a) shows the well-distributed 30B nanoclay particles inside the rubber blends. The thickness was in the range 2–3 nm, which indicated predominant exfoliation of the clay galleries and confirmed the earlier XRD results. The corresponding three-dimensional image of this sample in Figure 2(b) gave further insight into the clay dispersion in the blended rubber matrix. The distribution of 30B was also clearer from the three-dimensional image of the corresponding sample.

On the other hand, in the case of the NA-filled sample [Fig. 2(c)], the clay was locally confined to smaller areas and not distributed evenly in the blend. The thickness of one representative tactoid,

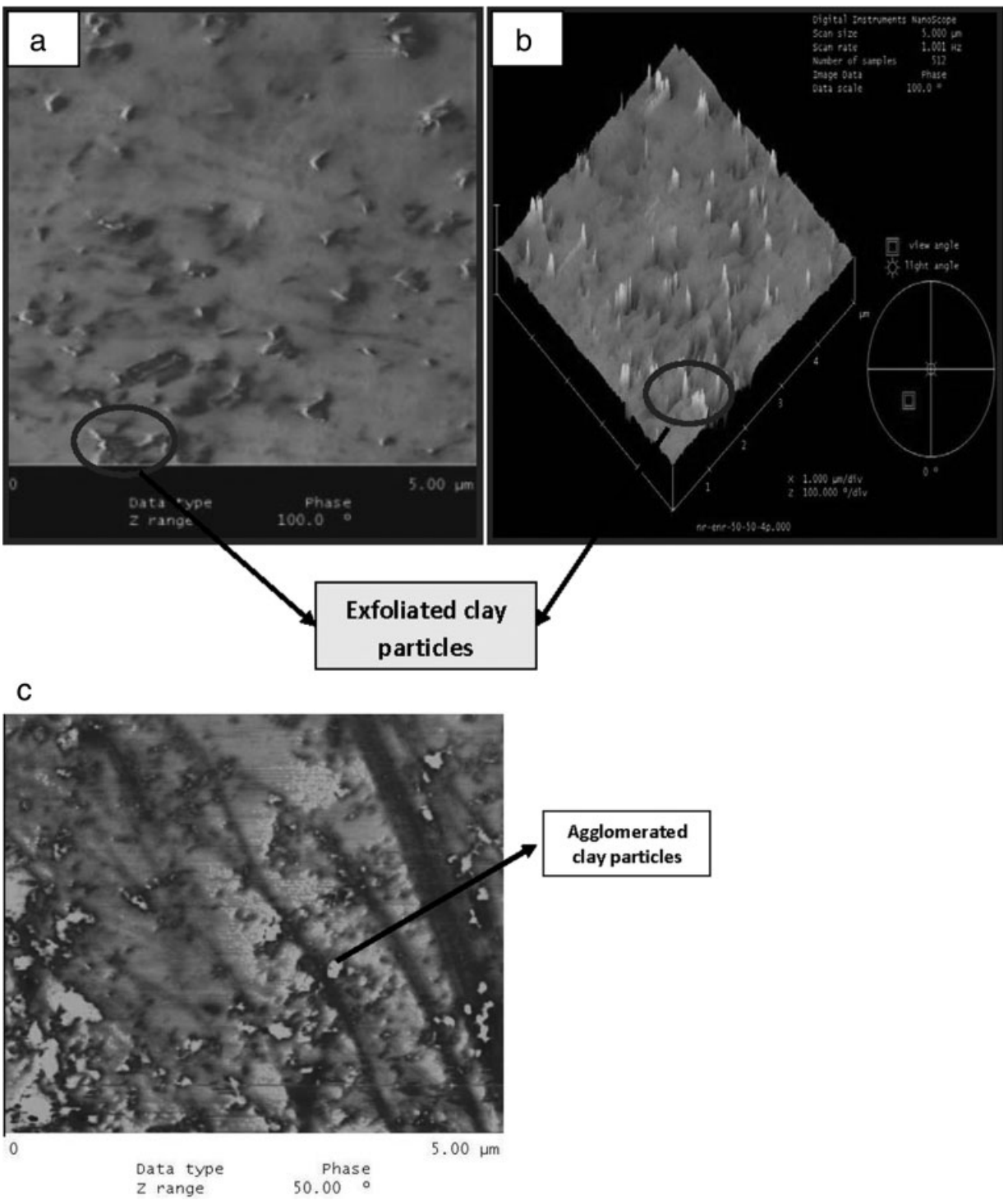

Figure 2 AFM images: (a,b) phase and height images of an NR/BR (50 : 50) blend with 4 phr 30B and (c) phase image of an NR/BR (50 : 50) blend with 4 phr NA.

marked in Figure 2(c), was 30 ± 5 nm. In all of the pictures, the darker phase corresponds to the lower modulus rubber, that is, ENR (as depicted from the Mooney viscosity measurements in Table I) in the blend. 30B is predominantly seen in the darker phase/interface regions, whereas the more aggregated NA is in also the darker phase, that is, inside the ENR phase, which was also supported by DMA (discussed next).

Dynamic mechanical measurements

Figure 3(a) shows the tan δ plots of the 50 : 50 NR/ENR blends containing various concentrations of

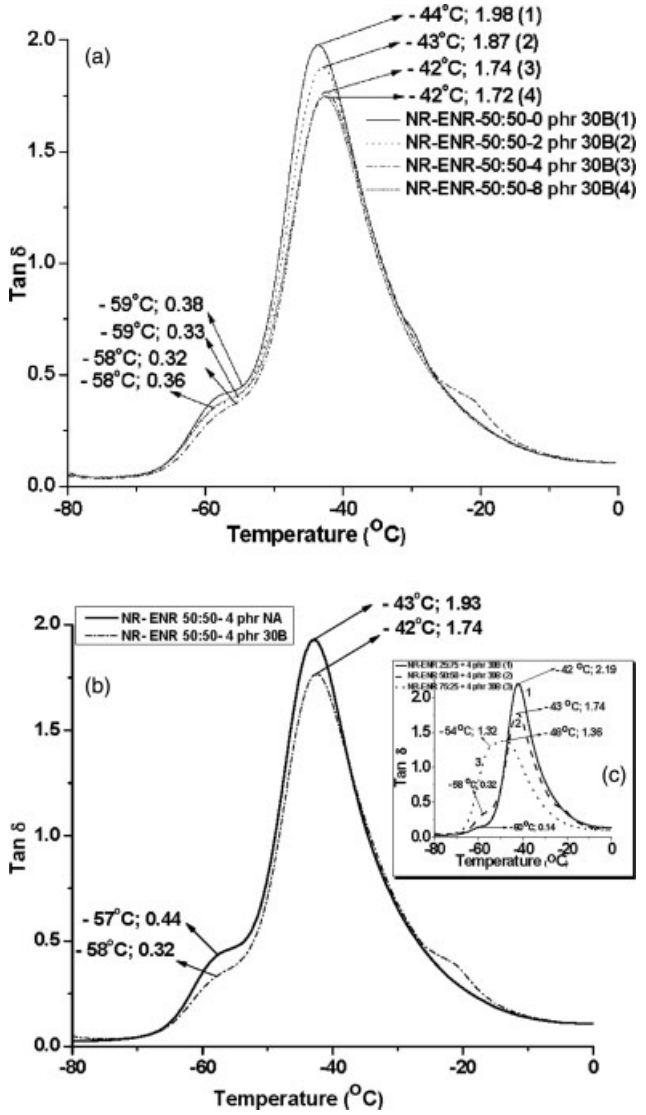

Figure 3 Tan δ–temperature plots of (a) 50 : 50 NR/ENR-50 blends with various 30B concentrations, (b) 50 : 50 NR/ENR blends with 4 phr NA and 30B, and (c) NR/ENR blends with 4 phr 30B and different blend ratios.

30B. The two tan δ peaks for each sample designate both the NR (peak at lower temperature) and the ENR (peak at relatively higher temperature) phases in the immiscible blends. The ENR peak was much larger than the NR peak, which indicated more damping effects due to the pendant epoxy groups. The addition of clay affected both these tan δ peaks, which indicated migration of the filler in both of these phases. The interaction of clay particles with these rubber molecules (both intercalation and exfoliation) suppressed the segmental mobility. The glass-transition temperature (T_g; i.e., tan δ peak temperature) values also marginally shifted to a higher temperature region because of these interactions with the rubber molecules. Maximum dampening occurred with a concentration of 4 parts of clay. Figure 3(b) demonstrates the importance of clay modification on the formation of interactive clay–rubber hybrids; the nanoclay (30B) suppressed the tan δ peaks quite significantly compared to the unmodified clay (NA). The decrease in peak height at the ENR phase was slightly more than that in the NR phase, which may have been due to better interaction between the epoxy groups of ENR and the amine surfactants in 30B. We expect that the shearing at 100°C was able to cause the cationic opening of the epoxy groups in ENR, which enhanced the interaction between the rubber and 30B. Also, the low Mooney viscosity of ENR compared to NR (Table I) may have helped favor the migration of the clay particles in the former, as also shown in Figure 2(a–c) (AFM plots).

The distribution of 30B and NA in the 50 : 50 NR/ENR-50 blends (R) was calculated as follows:[34]

$$R = \frac{(\tan \delta g)_{\max} - (\tan \delta f)_{\max}}{(\tan \delta g)_{\max}} \quad (1)$$

where $(\tan \delta)_{\max}$ is the maximum value of tan δ and g and f represent the gum and filled systems, respectively. $(\tan \delta)_{\max}$ was obtained directly from the DMA data. The term R was correlated to the filler to polymer weight fraction (w) as follows:

$$R = \alpha w \quad (2)$$

where α represents the polymer–filler interaction parameter. The weight fraction of the filler in the particular phase of the blend (w'_1) was determined as follows:

$$w'_1 = \frac{R'_1 R_2 w}{R'_1 R_2 + R_1 R'_2} \quad (3)$$

where R_1 is the distribution of clay for NR and NR + clay system, R_2 is the distribution of clay for ENR and ENR + clay system, R'_1 is the distribution of clay for NR phase in NR/ENR blend in addition to clay, R'_2 is the distribution of clay for ENR phase in NR/ENR blend in addition to clay.

The multiplication of w'_1 and weight fraction of filler in the ENR phase for NR/ENR blends (w'_2) thus obtained by 100 gave the percentage of the filler incorporated into rubber phases 1 and 2, respectively. With these equations, the amounts of 30B and NA present in the NR and ENR phases were

TABLE II
Distribution of Nanoclays in ENR and NR Phases in the 50 : 50 NR/ENR Blends

50 : 50 NR/ENR-50 blend	30 B (phr)	NA (phr)
NR phase	1.7 (42%)	0.3 (7%)
ENR phase	2.3 (58%)	3.7 (93%)

calculated, and the results are shown in Table II. The DMA plots of the individual rubbers with 30B and NA are not displayed separately for clarity. Both 30B and NA preferentially migrated toward the ENR phase rather than the NR phase. This was attributed to the low viscosity of the ENR phase. The higher polarity of NA was responsible for the better interaction with the pendant epoxy groups of the ENR phase, which also caused a comparatively higher migration of NA toward the ENR phase than that of 30B. The same trend was found with the volume fraction of the filler instead of the weight fraction.

Figure 3(c) shows the tan δ plots of different NR/ENR blends (25 : 75, 50 : 50, and 75 : 25), all loaded with 4 parts of 30B. Changing the blend ratio changed the intensity of both the NR and ENR tan δ peaks; a lower NR proportion in the blend resulted in much smaller peaks, whereas a higher proportion did the reverse. The most interesting observation was the gradual merging of the tan δ peaks the proportion of ENR in the blend in the presence of 30B was decreased. In fact, in the 75 : 25 NR/ENR blend composition, it was very difficult to identify the two T_g values. The same phenomenon did not occur in the absence of any nanoclay in the blend. 30B, therefore, definitely improved the miscibility between the NR and ENR and acted as a surfactant in the blend. These are unique observations that have not been reported before.

Mechanical properties

Figure 4 shows the tensile properties of the 50 : 50 NR/ENR blend nanocomposites. The tensile strength was better as the nanoclay loading (30B) was increased in the blends. The percentage increase in the maximum tensile stress (F_{max}) for the nanocomposites was calculated from the figure. The values are reported in Table III. There was an almost 55% increase in the tensile strength. Similarly, the tear strength was enhanced by 34% The tensile modulus, especially at low strain (<50%), was tremendously improved after nanoclay addition, which may possibly have been due to the interaction between the epoxy and the amine, as mentioned earlier. The elongation at break values did not follow any trend in any of these samples.

TABLE III
Increments in F_{max} and Tear Strength with Various 30B Contents in the 50 : 50 NR/ENR-50 Blends

Loading	Increment in F_{max} (%)	Increment in tear strength (%)
2 phr 30B	14	13
4 phr 30B	40	29
8 phr 30B	55	34
4 phr NA	−4	−2

30B showed significant improvement in both the tensile and tear properties because of the relatively better dispersion of 30B (Table II) in the rubber phases compared to NA and also the better interaction between them. A comparatively more aggregated structure of the latter reduced the available surface for interaction with the rubber chains as well. These, in fact, produced negative changes in the mechanical properties, as reported in Table III.

NR/BR–clay hybrid composites

XRD analysis

Figure 5(a) shows the X-ray diffractograms of the 50 : 50 NR/BR blends containing different concentrations

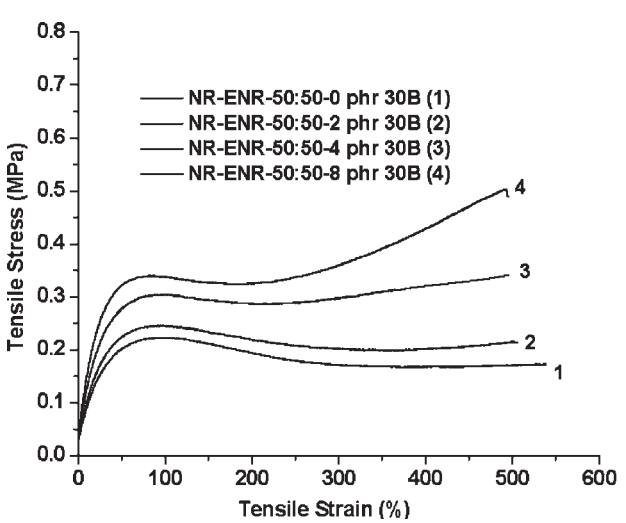

Figure 4 Stress–strain curves for 50 : 50 NR/ENR-50 blends with various 30B contents.

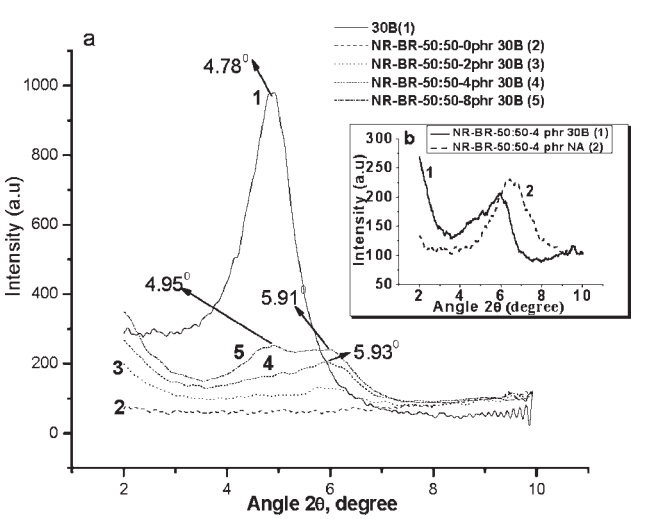

Figure 5 XRD patterns for (a) 50 : 50 NR/BR blends with 0, 2, 4, or 8 phr 30B and (b) 50 : 50 NR/BR blends with 4 phr 30B and NA, respectively.

of 30B. 30B showed a strong diffraction peak at $2\theta = 4.78^\circ$; this showed good concurrence with the literature values.[30] At lower concentrations of 30B, neither any significant peak shift nor any new diffraction peak was observed. This may possibly have been due to the destruction of the clay lamellas inside the blended matrix. A low volume concentration of the clay may have also resulted in the low intensity of the hybrid nanocomposites as well. However, at higher concentrations (4- and 8-phr loading), there was a small peak in the range 5.91–5.93°. A small peak at 4.95° was also observed at 8-phr concentration. These simply indicated that the clay layers were intercalated at a higher

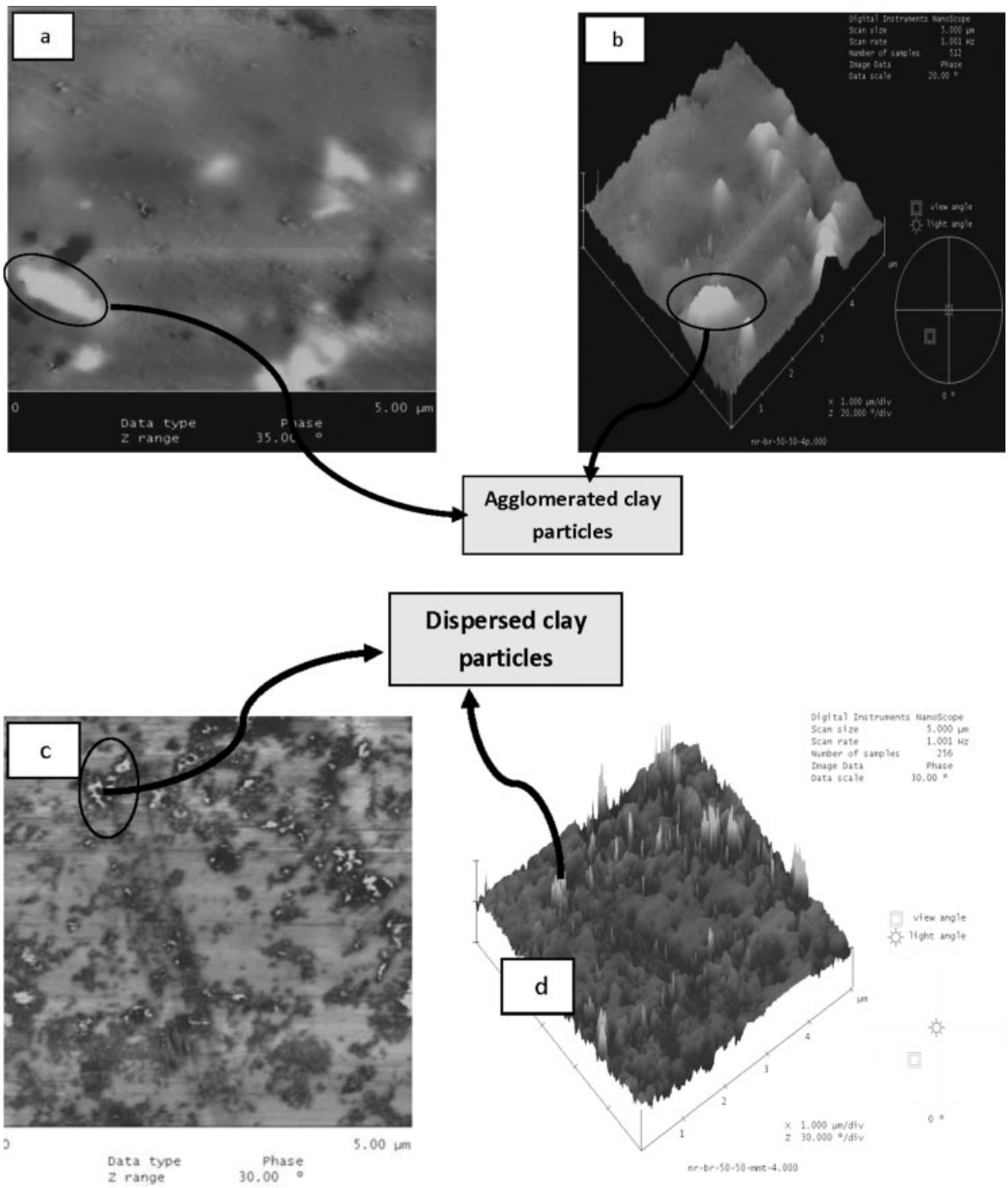

Figure 6 AFM images: (a,b) phase and height images of an NR/BR (50 : 50) blend with 4 phr 30B and (c,d) phase and height images of an NR/BR (50 : 50) blend with 4 phr NA.

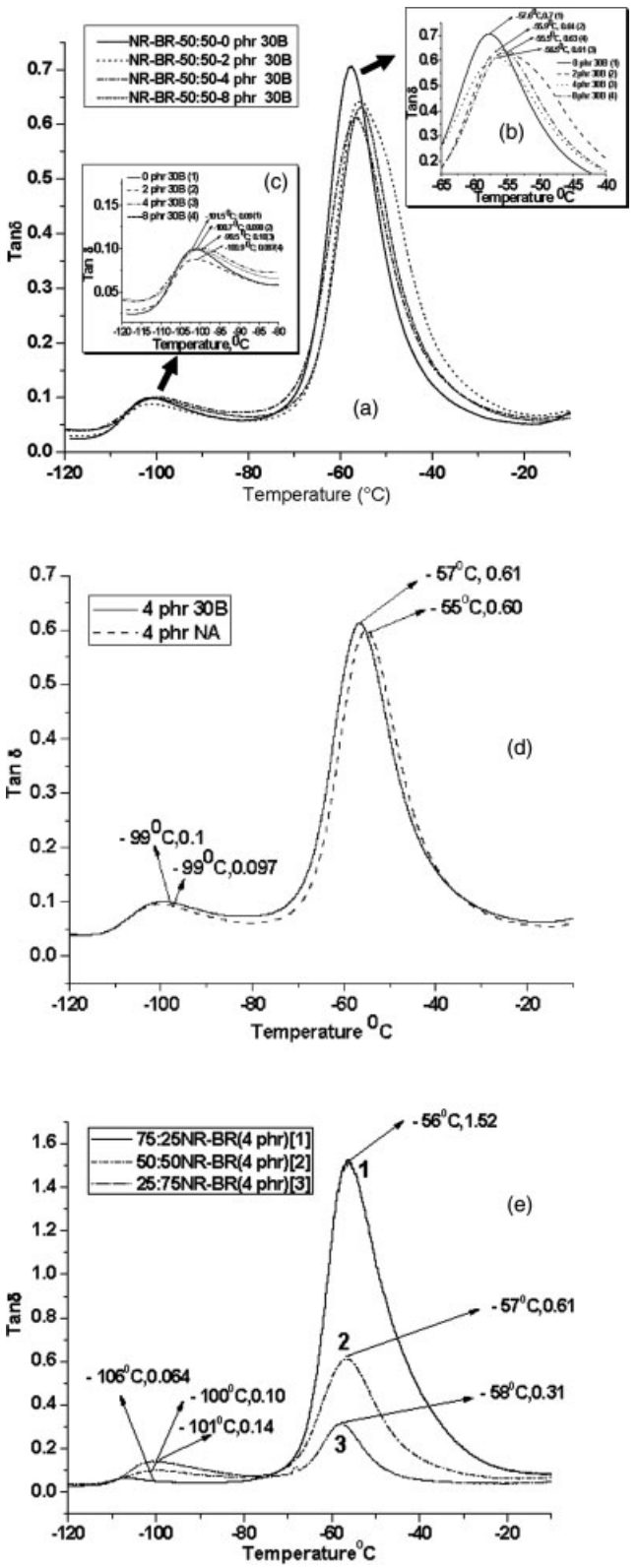

Figure 7 (a) Tan δ–temperature plots of NR/BR (50 : 50) blends with different concentrations of 30B, (b,c) magnified DMA plots of the NR and BR phases in the 50 : 50 NR/BR blends, (d) tan δ–temperature plots of NR/BR (50 : 50) blends with 4 phr NA and 30B, and (e) tan δ–temperature plots of different NR/BR blends with 4 phr 30B.

concentration. Figure 5(b) shows the XRD patterns for the 50 : 50 NR/BR blends containing 4 phr 30B and NA, respectively. The diffraction peaks assigned to NA were slightly higher in intensity than 30B and are shown clearly in the figure.

Morphology analysis

The distribution of the lamellas of 30B in the rubber matrix is shown in Figure 6(a,b). A major fraction of the clay migrated toward the NR phase and produced an aggregated morphology. The average width of the marked particle was about 350 nm. On the other hand, an almost uniform distribution of NA in the blended matrix was observed, as shown in Figure 6(c,d). The average width of the tactoids was significantly low, about 20 nm. Although a majority of the particles displayed intercalation, these were well distributed inside the rubber matrix compared to the organically modified clay particles.

Dynamic mechanical thermal analysis

Figure 7(a–c) shows the tan δ versus temperature for the nonpolar–nonpolar 50 : 50 NR/BR blends at different clay concentrations. NR/BR formed an immiscible blend and showed two different T_g values (two tan δ peaks). The addition of clay affected both of the peaks. The amplified peaks are shown separately in the inset [Fig. 7(b) for NR and Fig. 7(c) for BR]. At a very high clay concentration, that is, 8 phr, the peak height slightly increased, which possibly indicated the prior attainment of the saturation level (at 4 phr). This was similar to the results obtained for the NR/ENR system in the first part of this article. Interestingly, the comparative plot between 4 parts of 30B and NA in the NR/BR 50 : 50 blend system in Figure 7(d) showed a greater peak lowering effect with NA than with 30B. The observation that the 30B clay had less of an effect on T_g shifting in the NR/BR blend probably derived from its high incompatibility with either of the phases. Also, a minor shift of 1°C was observed in the NR phase in the blend as well. The clay distributions in different rubber phases in the blend were calculated with eqs. (1)–(3), and the corresponding results are shown in Table IV.

TABLE IV
Distribution of Nanoclays in the NR and BR Phases in the 50 : 50 NR/BR Blends

Phase	30B (phr)	NA (phr)
NR	3.4 (85%)	2.2 (55%)
BR	0.6 (15%)	1.8 (45%)

TABLE V
Increments in F_{max} and Tear Strength with Various 30B Contents in the 50 : 50 NR/BR Blends

Loading	Increment in F_{max} (%)	Increment in tear strength (%)
2 phr 30B	17	3
4 phr 30B	33	9
8 phr 30B	29	7
4 phr NA	29	20

The data show that the distribution was apparently even with NA, but 30B exhibited a remarkable difference in its distribution: almost all of the added 30B migrated to the NR phase in the blend. Also, both of the clays migrated toward NR, which in comparison to the NR/ENR blend, was contradictory (Table II). The data in Table IV probably shows that the migration of NA in the blend was primarily controlled by the individual viscosities of the rubber phases: NR showed a clearly lower viscosity than BR at the processing stage (Table I), which eased diffusion into the clay. 30B, on the other hand, despite its more hydrophobic nature, showed a slightly lower affinity toward BR, which may again have been due to the viscosity factor. The relative polarities of the phases would also have been a stronger determinant of clay partitioning. Viscosity may, however, have had a kinetic effect because of phase deformation during mixing.

Figure 7(e) shows the tan δ plots for different NR/BR blends containing 4 parts of 30B, and this time, 30B did not show any compatibilizing effects on the NR and BR phases, as was observed in the case of the NR/ENR blends [Fig. 3(c)]. Also, rubber phase/clay interaction may have also been the cause of the T_g peak shift toward each other.

Mechanical properties

The tensile stress–strain plots of the green (unvulcanized) hybrid composites were analyzed. The increment in the F_{max} value and the tear strength are tabulated in Table V. The addition of nanoclay improved both the properties; maximum improvement was noticed with a 4-phr concentrations because of the comparatively better dispersion in the rubber matrix than with other clay concentrations. NA, on the other hand, showed a relatively better improvement than that achieved with 30B. A relatively finer and uniform distribution of the clay particles imparted better properties of the unvulcanized compounds.

CONCLUSIONS

It was clearly demonstrated that the distribution of clay in the rubber phases in immiscible rubber–rubber blends (NR/ENR and NR/BR) primarily varied with the nature of the rubbers, their viscosity, and the nature of the clay. In a polar–nonpolar blend system, the distribution was predominantly controlled by the clay–rubber interactions. NA, with a higher polarity, migrated more into the polar rubber phase (ENR), whereas the reverse was true for 30B, which was comparatively less polar and organophilic. The study also showed that the organically modified nanoclay also played the role of a surfactant in the polar–nonpolar rubber–rubber blends such as NR and ENR. The results are even interesting when a relatively nonpolar rubber blend such as NR/BR is considered. Although NR is slightly more polar than BR, the governing factor for the distribution of the nanofiller was the viscosity of the individual phases, as no specific interaction was possible in this case. NA showed better uniform distribution among both the phases compared to 30B, which clearly showed big aggregated clusters, mainly inside the NR phase.

References

1. Schmidt, H. J. Non Cryst Solids 1985, 73, 681.
2. Novak, B. M. Adv Mater 1993, 5, 422.
3. Sadhu, S.; Bhowmick, A. K. J Appl Polym Sci 2004, 92, 698.
4. Sadhu, S.; Bhowmick, A. K. Rubber Chem Technol 2005, 78, 321.
5. Lan, T.; Pinnavaia, T. J. J Chem Mater 1994, 6, 2216.
6. Agag, T.; Takeichi, T. Polymer 2000, 41, 7083.
7. Hong, S. H.; Kim, B. H.; Joo, J.; Kim, J. W.; Choi, H. J. Curr Appl Phys 2001, 1, 447.
8. Fornes, T. D.; Yoon, P. J.; Hunter, D. L.; Keskkula, H.; Paul, D. R. Polymer 2002, 43, 5915.
9. Kim, B. H.; Jung, J. H.; Hong, S. H.; Kim, J. W.; Choi, H. J.; Joo, J. Curr Appl Phys 2001, 1, 112.
10. Chen, T. K.; Tien, Y. I.; Wei, K. H. Polymer 2000, 41, 1345.
11. Tortora, M.; Gorrasi, G.; Vittoria, V.; Gallib, G.; Ritrovati, S.; Chiellinim, E. Polymer 2002, 43, 6147.
12. Sadhu, S.; Bhowmick, A. K. J Polym Sci Part B: Polym Phys 2004, 42, 1573.
13. Kojima, Y.; Fujushima, A.; Usuki, A.; Okada, A.; Kurauchi, T. Mater Sci Lett 1993, 12, 889.
14. Chie, Y. C.; Ma, C. C. M.; Liu, F. Y.; Chiang, C. L.; Riang, L.; Yang, J. C. Eur Polym J 2008, 44, 1003.
15. Gilman, J. W. Appl Clay Sci 1999, 15, 31.
16. Tidjani, A.; Wilkie, C. A. Polym Degrad Stab 2001, 74, 33.
17. Bourbigot, S.; Devaux, E.; Flambard, X. Polym Degrad Stab 2002, 75, 397.
18. Zhua, J.; Startb, P.; Mauritzb, K. A.; Wilkiea, C. A. Polym Degrad Stab 2002, 77, 253.
19. Guo, Z.; Kim, T. Y.; Lei, K.; Pereira, T.; Jonathan, G. S.; Hahn, H. T. Compos Sci Technol 2008, 68, 164.
20. Sinha Ray, S.; Okamoto, M. Prog Polym Sci 2003, 28, 1539.
21. Kocsis, J. K.; Wu, C. M. Polym Eng Sci 2004, 44, 1083.
22. Vaia, R. A.; Vasudevan, S.; Krawiec, W.; Scanlon, L. G.; Giannelis, E. P. Adv Mater 1995, 7, 154.
23. Giannelis, E. P. Adv Mater 1996, 8, 29.
24. Bandyopadhyay, A.; Maiti, M.; Bhowmick, A. K. Mater Sci Technol 2006, 22, 818.

25. Bhattacharya, M.; Maiti, M.; Bhowmick, A. K. Rubber Chem Technol 2008, 81, 384.
26. Sadhu, S.; Bhowmick, A. K. Rubber Chem Technol 2005, 78, 321.
27. Maiti, M.; Mitra, S.; Bhowmick, A. K. Polym Degrad Stab 2008, 99, 188.
28. Maiti, M.; Sadhu, S.; Bhowmick, A. K. J Polym Sci Part B: Polym Phys 2004, 42, 4489.
29. Maiti, M.; Sadhu, S.; Bhowmick, A. K. J Appl Polym Sci 2006, 603, 101.
30. Maiti, M.; Bhattacharya, M.; Bhowmick, A. K. Rubber Chem Technol 2008, 81, 384.
31. Arroyo, M.; López-Manchado, M. A.; Valentín, J. L.; Carretero, J. Compos Sci Technol 2007, 67, 1330.
32. Zhu, J.; Wang, X.; Fangfang, T.; Xue, G.; Chen, T.; Sun, P.; Jin, Q.; Ding, D. Polymer 2007, 48, 7590.
33. Maiti, M.; Bhowmick, A. K. Polymer 2006, 47, 6156.
34. Maiti, S.; De, S. K.; Bhowmick, A. K. Rubber Chem Technol 1992, 65, 293.